Report

Current Biology

Moonwalker Descending Neurons Mediate Visually Evoked Retreat in *Drosophila*

Highlights

- Optogenetic activation of LC16 or MDN cells triggers backward locomotion
- Optogenetic activation of LC16 is sufficient to elicit calcium responses in MDNs
- Silencing the activity of MDNs eliminates LC16-triggered backward turning
- Asymmetric activation of MDNs induces directed backward turns

Authors

Rajyashree Sen, Ming Wu, Kristin Branson, Alice Robie, Gerald M. Rubin, Barry J. Dickson

Correspondence

dicksonb@janelia.hhmi.org

In Brief

Sen et al. demonstrate that a specific population of visual projection neurons, the lobula columnar 16 (LC16) cells, acts via the moonwalker descending neurons (MDNs) to trigger retreat in *Drosophila*.

Sen et al., 2017, Current Biology *27*, 766–771
March 6, 2017
http://dx.doi.org/10.1016/j.cub.2017.02.008

CellPress

CellPress

Current Biology
Report

Moonwalker Descending Neurons Mediate Visually Evoked Retreat in *Drosophila*

Rajyashree Sen,[1] Ming Wu,[1,2] Kristin Branson,[1] Alice Robie,[1] Gerald M. Rubin,[1] and Barry J. Dickson[1,3,*]
[1]Janelia Research Campus, Howard Hughes Medical Institute, 19700 Helix Drive, Ashburn, VA 20147, USA
[2]Present address: Salubris Biotherapeutics, Gaithersburg, MD 20878, USA
[3]Lead Contact
*Correspondence: dicksonb@janelia.hhmi.org
http://dx.doi.org/10.1016/j.cub.2017.02.008

SUMMARY

Insects, like most animals, tend to steer away from imminent threats [1–7]. *Drosophila melanogaster*, for example, generally initiate an escape take-off in response to a looming visual stimulus, mimicking a potential predator [8]. The escape response to a visual threat is, however, flexible [9–12] and can alternatively consist of walking backward away from the perceived threat [11], which may be a more effective response to ambush predators such as nymphal praying mantids [7]. Flexibility in escape behavior may also add an element of unpredictability that makes it difficult for predators to anticipate or learn the prey's likely response [3–6]. Whereas the fly's escape jump has been well studied [8, 9, 13–18], the neuronal underpinnings of evasive walking remain largely unexplored. We previously reported the identification of a cluster of descending neurons—the moonwalker descending neurons (MDNs)—the activity of which is necessary and sufficient to trigger backward walking [19], as well as a population of visual projection neurons—the lobula columnar 16 (LC16) cells—that respond to looming visual stimuli and elicit backward walking and turning [11]. Given the similarity of their activation phenotypes, we hypothesized that LC16 neurons induce backward walking via MDNs and that turning while walking backward might reflect asymmetric activation of the left and right MDNs. Here, we present data from functional imaging, behavioral epistasis, and unilateral activation experiments that support these hypotheses. We conclude that LC16 and MDNs are critical components of the neural circuit that transduces threatening visual stimuli into directional locomotor output.

RESULTS AND DISCUSSION

In our first series of experiments, we revisited the neuronal activation phenotypes of lobula columnar 16 (LC16) and moonwalker descending neuron (MDN) cells by acutely depolarizing them using a red-light-activated cation channel, CsChrimson [20], in an optogenetic behavioral assay. We used two different split-GAL4 driver lines that label the identical LC16 population (LC16-1 and LC16-2 GAL4s) and three different lines that label the identical MDN cells (MDN-1, MDN-2, and MDN-3 GAL4s; see the list of genotypes in the Supplemental Experimental Procedures). Bilateral activation of either LC16 cells or MDNs elicited backward locomotion, as previously observed [11, 19], but a closer examination revealed subtle differences between the LC16- and MDN-triggered motor programs (Figure 1). In order to quantify these behaviors, we used computer vision software to extract two distinct features of locomotion: translation and rotation (see the Supplemental Experimental Procedures). During the 2 s stimulation window, LC16 cells triggered transient backward locomotion that included a strong turning component—eventually leading the fly to resume forward walking in a direction different from its original heading (Figures 1A–1C; Movie S1). Upon LC16 activation, the resumption of forward locomotion would often begin during the 2 s light stimulation. By contrast, MDNs triggered slower, straight or slightly curved backward walking that persisted until the end of the stimulation period (Figures 1A–1C; Movie S1).

We used hysteresis-based thresholds [21, 22] to define six distinct behavioral states based on translational and angular velocities: straight backward walking, backward turning, straight forward walking, forward turning, stall, and pivot (i.e., turning without translation; see the Supplemental Experimental Procedures). Consistent with our qualitative observation, we observed that flies in which LC16 was activated predominantly showed backward turning and pivots, whereas flies with MDNs activated showed substantially more straight backward walking (Figures 1D and S1).

Next we asked whether LC16 could trigger neuronal responses in MDNs. We optogenetically activated the LC16 neuronal population with CsChrimson while simultaneously imaging calcium transients in the dendritic arbors of MDNs using GCaMP6m [23] (Figure 2A). In an explanted central nervous system (CNS), optogenetic activation of LC16 cells was sufficient to trigger calcium responses in MDNs (Figures 2B and 2C). The response was mostly abolished by bath application of mecamylamine—an inhibitor of cholinergic synaptic transmission (Figures 2B and 2C). These results suggest that LC16 neurons activate MDNs via an excitatory cholinergic input. This input is unlikely to be a direct synaptic connection since the arborizations of LC16 and MDN cells do not overlap (Figure 2A; Movie S2).

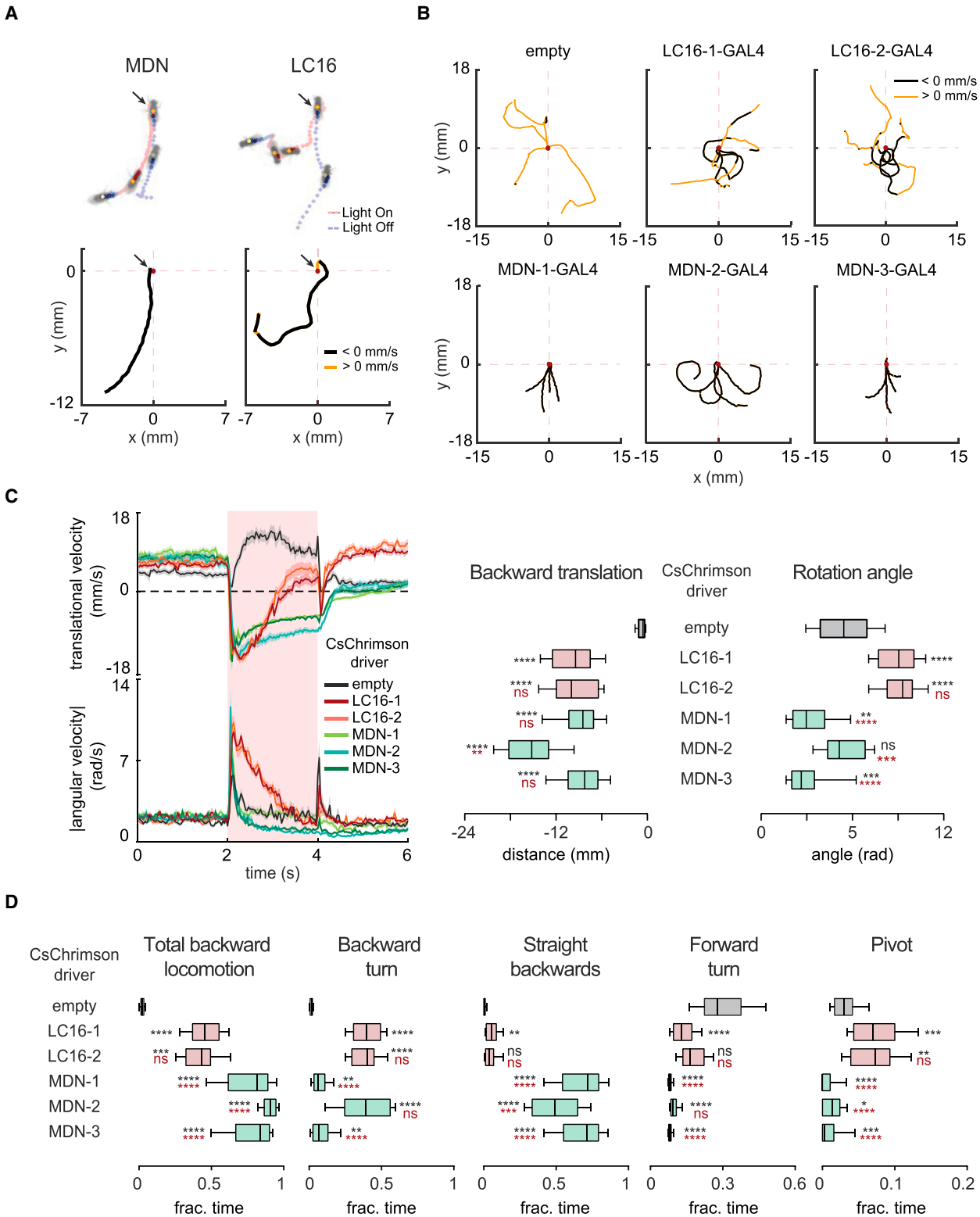

Figure 1. Similar but Distinct Features of Backward Locomotion upon Optogenetic Activation of MDNs or LC16 Cells

(A) Representative motion traces upon optogenetic activation of MDNs and LC16 cells, using the *MDN-2* and *LC16-1* split-GAL4 driver lines, respectively, to drive the expression of *UAS-CsChrimson*. Top: trajectories before, during, and after stimulation. Blue traces, light off; red traces, light on. Arrows indicate position at start of stimulation. Bottom: trajectories of the same flies during the 2 s stimulation window, now color-coded for backward (<0 mm/s) or forward (>0 mm/s) translational velocity. Translational velocity in this and other panels is defined as the projection of the fly's locomotion vector onto its orientation direction.

(legend continued on next page)

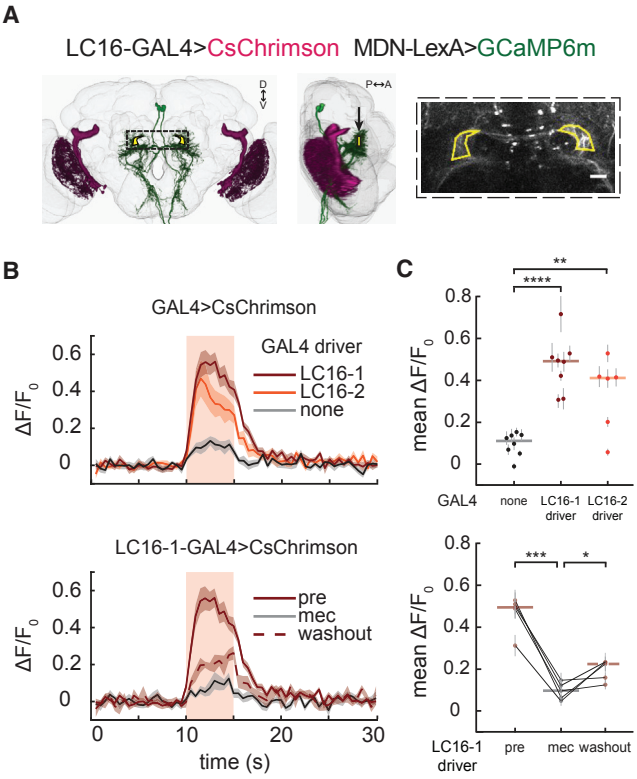

Figure 2. Optogenetic Activation of LC16 Cells Elicits Calcium Responses in MDNs

(A) Left and center: schematic of the brain showing LC16 neurons (magenta, expressing CsChrimson) and MDNs (green, expressing GCaMP6m). Yellow polygons within the dotted rectangle show regions of interest for functional imaging. Right: regions of interest overlaid on MDN arbors in a projection image of a representative sample. Scale bar, 20 μm.

(B) Top: time series for calcium responses in MDNs upon optogenetic activation of LC16 cells (n = 6–8 flies). Bottom: responses of MDNs to LC16 activation upon application and washout of mecamylamine (n = 5 flies). Dark traces indicate mean of per-fly means (20 trials per fly, ten on each side of the brain) versus time, and envelopes indicate ±SEM.

(C) Top: per-fly means of average MDN $\Delta F/F_0$ values during 5 s of LC16 activation (n = 6–8 flies), shown in jitter plots in which each dot represents per-fly mean of 20 trials and whiskers represent ±SEM. Horizontal bars indicate median values. p values are for comparisons to no GAL4 control (unpaired Student's t test with Bonferroni correction). Bottom: quantification of responses upon application and washout of mecamylamine (mec; n = 5 flies). p values are for paired comparisons to mecamylamine-treated samples (paired Student's t test). See also Movie S2 and Tables S1 and S2.

Is MDN activity necessary for LC16-triggered backward locomotion? To address this question, we activated LC16 with CsChrimson in a background in which MDNs were inactivated by expression of the tetanus toxin light chain (TNT), an inhibitor of synaptic transmission [24]. As a positive control, we included flies in which TNT was expressed in LC16 rather than MDNs. As a negative control, we used flies in which an empty vector controlled TNT expression. We observed that the backward component of LC16-triggered retreat was dramatically reduced in all experimental and positive control genotypes, but not in the negative controls (Figure 3; Movie S3). The residual backward translation of the experimental flies was not significantly different from that of the positive control, suggesting that it reflects incomplete neuronal silencing with TNT rather than an MDN-independent component to LC16-triggered backward locomotion (Figures 3B–3D).

By contrast, the turning component resulting from LC16 activation was partially suppressed when MDNs were silenced (Figures 3C–3D; Movie S3), suggesting that LC16 neurons induce turning via both MDN-dependent and MDN-independent pathways. Quantification of the six behavioral states revealed that LC16-trigged backward turns were effectively and similarly suppressed by silencing of either MDNs or the LC16 cells themselves (Figures 3D and S2). The MDN-dependent pathway thus mediates the backward turns elicited by LC16 activation. Forward turns were more weakly and variably suppressed by MDN silencing (Figure 3D), suggesting that they rely primarily on the MDN-independent pathway. Pivots were increased upon both MDN and LC16 silencing (Figure 3D), perhaps in both cases as an indirect consequence of the inability to retreat.

There are four MDN cells, two on each side of the CNS, with axons that project contralaterally to all three leg neuropils of the thoracic ganglia [19]. We speculated that asymmetric activation of the left and right MDNs might result in backward turning. To address this possibility, we applied a genetic approach to stochastically activate subsets of the four MDN cells [11] (see the Supplemental Experimental Procedures). In individual flies, the stochastically activated cells can be anatomically identified and correlated to the fly's behavior (Figures 4A–4C; Movie S4). We found that, overall, the extent of backward translation correlated with the total number of MDNs activated and the amount of turning correlated with the asymmetry of activation (Figure 4C). Asymmetric MDN activation consistently favored backward turning to the contralateral side (with respect to the location of the MDN soma in the brain). These results suggest that each of the four MDNs can act independently and that collectively they control both the magnitude and direction of backward locomotion.

In conclusion, our results suggest that LC16 cells and MDNs mediate visually evoked retreat via an excitatory feedforward circuit (Figure 4D). The four MDN cells can elicit a range of related motor outputs, depending on the pattern of their

(B) Representative trajectories during the 2 s stimulation window of four flies for each of the various cell-type specific drivers.

(C) Left: translational and angular velocities versus time. Dark traces indicate mean of per-fly means (five trials per fly), and envelopes indicate ±SEM. Red rectangles in this and other panels signify optogenetic stimulation with red light. Right: per-fly mean, over five trials, of total backward translation distances and rotation angles during 2 s of optogenetic stimulation (n = 26–56 flies). Box-and-whisker plots in this and other panels show 10th, 25th, 50th, 75th, and 90th percentiles. Statistical significance was assessed using the Kruskal-Wallis test ($p < 0.0001$ for both panels), followed by Dunn's post hoc test for pairwise comparisons against the empty GAL4 (black) and LC16-1 (red) controls. In this and other panels, ****$p < 0.0001$, ***$p < 0.001$, **$p < 0.01$, and *$p < 0.05$; ns, not significant.

(D) Per-fly mean, over five trials, of the fraction of time spent in the indicated behavioral states during the 2 s window of optogenetic activation. Kruskal-Wallis tests ($p < 0.0001$ for all panels) were followed by Dunn's post hoc test for pairwise comparisons against empty GAL4 (black) and LC16-1 (red) controls. Data for straight forward and stalled states are shown in Figure S1.

See also Movie S1.

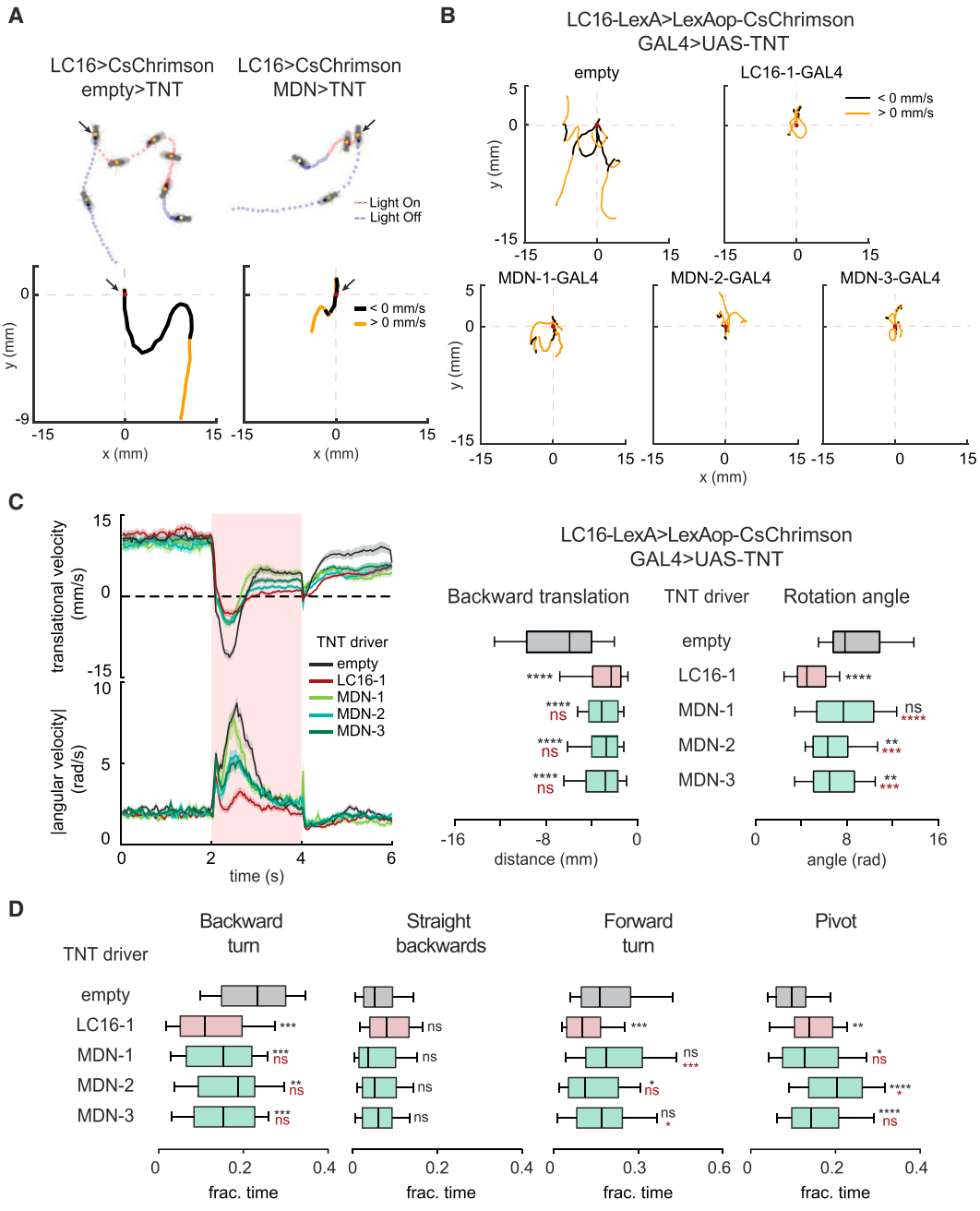

Figure 3. LC16 Neurons Act via MDNs to Trigger Backward Locomotion

(A) Top: optogenetic activation of LC16 cells in combination with either *MDN-3* or the empty GAL4 control driving expression of TNT. Motion traces of representative flies are indicated. Blue traces, light off; red traces, light on. Arrows indicate position at the start of optogenetic stimulation. Bottom: trajectories during the 2 s window of optogenetic stimulation, now color-coded for backward (<0 mm/s) or forward (>0 mm/s) translational velocity.

(B) Representative trajectories of four flies for various genotypes used in the neuronal epistasis experiments. The traces include only the 2 s stimulus window.

(C) Left: translational and angular velocities versus time upon optogenetic stimulation of LC16 cells. Dark traces indicate mean of per-fly means (five trials per fly), and envelopes indicate ±SEM (n = 45–70 flies). Right: per-fly mean, over five trials, of total backward translation distances and rotation angles during the 2 s of optogenetic stimulation of LC16 cells. Statistical significance was assessed using the Kruskal-Wallis test ($p < 0.0001$ for both panels), followed by Dunn's post hoc test for pairwise comparisons against the empty GAL4 (black) and LC16-1 (red) controls.

(D) Per-fly mean, over five trials, of fraction of time spent in each behavioral state during the 2 s stimulus window. Kruskal-Wallis tests ($p < 0.0001$ for backward turn, forward turn, and pivot; $p = 0.07$ for backward straight) were followed by Dunn's post hoc test in pairwise comparisons against the negative (empty; black) and positive (LC16-1; red) controls. Data for forward straight and stalled states are shown in Figure S2.

See also Movie S3.

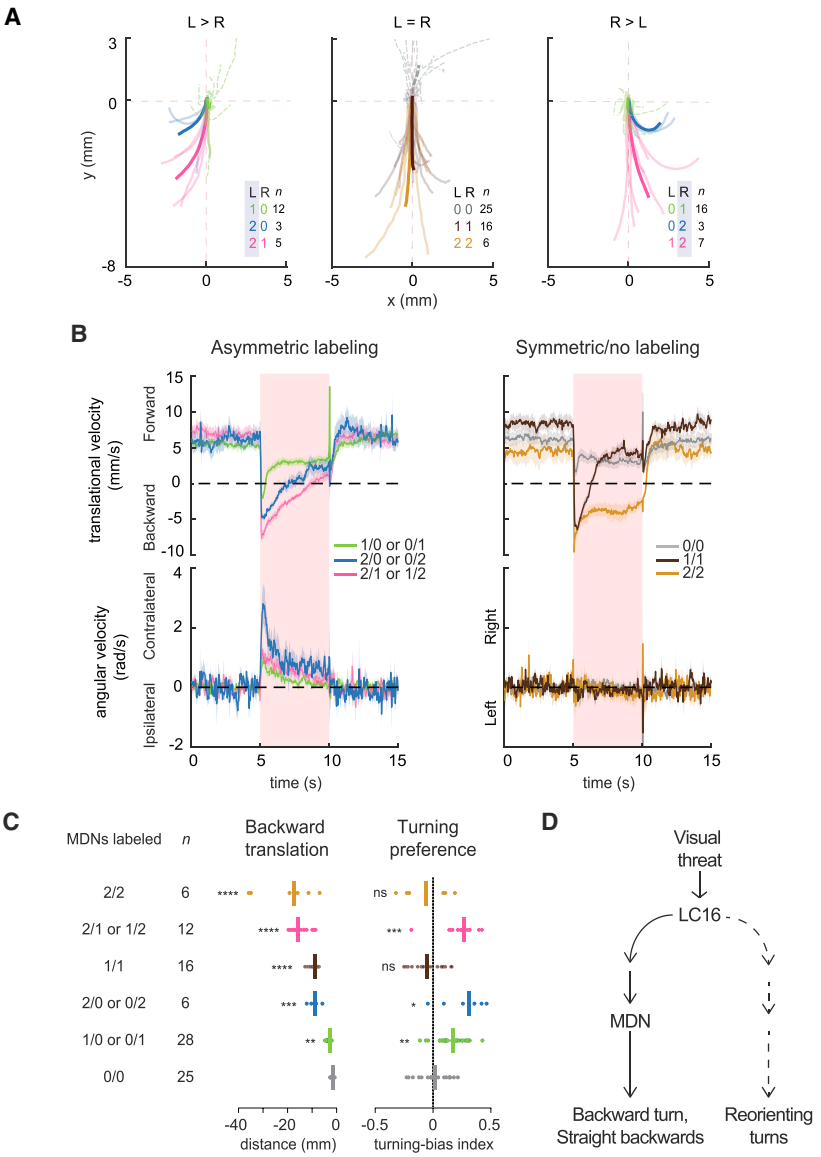

Figure 4. Asymmetric Activation of MDNs Causes Contralateral Backward Turns

(A) Trajectories of all flies during the first 1 s of MDN activation. Left: categories with more left (L) than right (R) MDN cells labeled. Middle: categories with no or an equal number of MDN cells labeled in the two brain hemispheres. Right: categories with more right than left MDN cells labeled. Per-fly mean trajectories over 15 trials (faded lines) and per-category mean trajectories (bold lines) are indicated. Solid and dotted lines indicate backward (<0 mm/s) and forward (>0 mm/s) translation, respectively. "*n*" indicates the number of flies tested in each category.

(B) Time series for stochastic activation of MDNs. Positive and negative values for translational velocity indicate forward and backward locomotion, respectively. Positive and negative values for angular velocity indicate contralateral and ipsilateral turns (with respect to the side where more MDNs were labeled), respectively, for asymmetric labeling classes, and right and left turns, respectively, for symmetric/no labeling classes. Dark traces indicate means of per-fly means (15 trials per fly), pooled from all flies of a given labeling category, and envelopes indicate ±SEM (n = 6–28 flies).

(C) Per-fly mean of backward translation distances and turning-bias indices for flies with varying numbers of MDNs activated (15 trials per fly). Vertical bars indicate median values. Turning-bias indices are defined as either the ratio of contralateral / (contralateral + ipsilateral) angular distances (with respect to the side where more MDN cells were labeled; asymmetric labeling) or as right / (left + right) angular distances (symmetric/no labeling). Ratios are normalized by subtraction of light-off turning preferences to correct for any inherent left-right bias in a given fly. A Kruskal-Wallis test ($p < 0.0001$ for both panels) was followed by Dunn's post hoc test of pairwise comparisons against the category with no activated MDN cells (0/0; p values indicated).

(D) Schematic showing the proposed roles of LC16 neurons and MDNs in visually evoked retreat in *Drosophila*.

See also Movie S4.

activity: symmetric activation of all four MDNs elicits straight backward walking, whereas asymmetric activation favors backward turning. Under natural conditions, a visual threat is likely to preferentially activate the ipsilateral LC16 cells, which we infer would lead to stronger activation of the ipsilateral MDNs and hence contralateral (evasive) turning. Even in the absence of pronounced asymmetry in LC16 activation, intervening circuits may introduce or amplify left-right differences to result in primarily unilateral MDN activation. We anticipate that MDNs also receive input from other sensory pathways. Mechanosensory cues, for example, might activate MDNs in response to a physical obstruction, and these too might differentially activate ipsilateral and contralateral MDNs to determine both the direction and extent of backward walking. The descending neurons that control forward walking and turning in *Drosophila* have not yet been identified, but once they are, it will be interesting to determine whether these cells employ an analogous logic to that of the MDNs to direct forward, rather than backward, walking and turning.

SUPPLEMENTAL INFORMATION

Supplemental Information includes Supplemental Experimental Procedures, two figures, two tables, and four movies and can be found with this article online at http://dx.doi.org/10.1016/j.cub.2017.02.008.

AUTHOR CONTRIBUTIONS

R.S. and M.W. performed the behavioral experiments. R.S. performed the antibody staining and the calcium imaging experiments and analyzed all data. K.B. generated the script for tracking fly directionality and contributed to the script for video analysis. A.R. advised the engineering of the optogenetic fly chamber and contributed to the video analysis script. R.S., M.W., and B.J.D. designed the experiments and wrote the manuscript. B.J.D. and G.M.R. supervised the project.

ACKNOWLEDGMENTS

We thank Barret Pfeiffer for pJFRC35; Heather Dionne for 28F07-LexAp65; Romain Franconville and Kaiyu Wang for assisting with the calcium imaging

experiments; Ines Ribeiro and Allen Lee for assisting in data analysis; William Rowell, Teri Ngo, and Jon-Michael Knapp for technical assistance; Aljoscha Nern, Yoshi Aso, Zhiyong Liu, and Wyatt Korff for technical advice; Vivek Jayaraman for CsChrimson stocks; and Steve Sawtelle, Igor Negrashov, and Jinyang Liu for engineering the optogenetic fly chamber. M.W. was a Helen Hay Whitney Postdoctoral Fellow. This work was funded by the Howard Hughes Medical Institute.

Received: October 14, 2016
Revised: January 20, 2017
Accepted: February 2, 2017
Published: February 23, 2017

REFERENCES

1. Tauber, E., and Camhi, J. (1995). The wind-evoked escape behavior of the cricket *Gryllus bimaculatus*: integration of behavioral elements. J. Exp. Biol. *198*, 1895–1907.
2. Kanou, M., Ohshima, M., and Inoue, J. (1999). The air-puff evoked escape behavior of the cricket *Gryllus bimaculatus* and its compensational recovery after cercal ablations. Zoolog. Sci. *16*, 71–79.
3. Domenici, P., Booth, D., Blagburn, J.M., and Bacon, J.P. (2008). Cockroaches keep predators guessing by using preferred escape trajectories. Curr. Biol. *18*, 1792–1796.
4. Domenici, P., Booth, D., Blagburn, J.M., and Bacon, J.P. (2009). Escaping away from and towards a threat: the cockroach's strategy for staying alive. Commun. Integr. Biol. *2*, 497–500.
5. Domenici, P., Blagburn, J.M., and Bacon, J.P. (2011). Animal escapology II: escape trajectory case studies. J. Exp. Biol. *214*, 2474–2494.
6. Card, G.M. (2012). Escape behaviors in insects. Curr. Opin. Neurobiol. *22*, 180–186.
7. Parigi, A., Porter, C., Cermak, M., Pitchers, W.R., and Dworkin, I. (2014). How predator hunting-modes affect prey behaviour: capture deterrence in *Drosophila melanogaster*. bioRxiv. http://dx.doi.org/10.1101/010330.
8. Allen, M.J., Godenschwege, T.A., Tanouye, M.A., and Phelan, P. (2006). Making an escape: development and function of the *Drosophila* giant fibre system. Semin. Cell Dev. Biol. *17*, 31–41.
9. von Reyn, C.R., Breads, P., Peek, M.Y., Zheng, G.Z., Williamson, W.R., Yee, A.L., Leonardo, A., and Card, G.M. (2014). A spike-timing mechanism for action selection. Nat. Neurosci. *17*, 962–970.
10. Gibson, W.T., Gonzalez, C.R., Fernandez, C., Ramasamy, L., Tabachnik, T., Du, R.R., Felsen, P.D., Maire, M.R., Perona, P., and Anderson, D.J. (2015). Behavioral responses to a repetitive visual threat stimulus express a persistent state of defensive arousal in *Drosophila*. Curr. Biol. *25*, 1401–1415.
11. Wu, M., Nern, A., Williamson, W.R., Morimoto, M.M., Reiser, M.B., Card, G.M., and Rubin, G.M. (2016). Visual projection neurons in the *Drosophila* lobula link feature detection to distinct behavioral programs. eLife *5*, e21022.
12. Herberholz, J., and Marquart, G.D. (2012). Decision making and behavioral choice during predator avoidance. Front. Neurosci. *6*, 125.
13. Tanouye, M.A., and Wyman, R.J. (1980). Motor outputs of giant nerve fiber in *Drosophila*. J. Neurophysiol. *44*, 405–421.
14. Hammond, S., and O'Shea, M. (2007). Escape flight initiation in the fly. J. Comp. Physiol. A Neuroethol. Sens. Neural Behav. Physiol. *193*, 471–476.
15. Card, G., and Dickinson, M.H. (2008). Visually mediated motor planning in the escape response of *Drosophila*. Curr. Biol. *18*, 1300–1307.
16. Card, G., and Dickinson, M. (2008). Performance trade-offs in the flight initiation of *Drosophila*. J. Exp. Biol. *211*, 341–353.
17. Fotowat, H., Fayyazuddin, A., Bellen, H.J., and Gabbiani, F. (2009). A novel neuronal pathway for visually guided escape in *Drosophila melanogaster*. J. Neurophysiol. *102*, 875–885.
18. de Vries, S.E., and Clandinin, T.R. (2012). Loom-sensitive neurons link computation to action in the *Drosophila* visual system. Curr. Biol. *22*, 353–362.
19. Bidaye, S.S., Machacek, C., Wu, Y., and Dickson, B.J. (2014). Neuronal control of *Drosophila* walking direction. Science *344*, 97–101.
20. Klapoetke, N.C., Murata, Y., Kim, S.S., Pulver, S.R., Birdsey-Benson, A., Cho, Y.K., Morimoto, T.K., Chuong, A.S., Carpenter, E.J., Tian, Z., et al. (2014). Independent optical excitation of distinct neural populations. Nat. Methods *11*, 338–346.
21. Robie, A.A., Straw, A.D., and Dickinson, M.H. (2010). Object preference by walking fruit flies, *Drosophila melanogaster*, is mediated by vision and graviperception. J. Exp. Biol. *213*, 2494–2506.
22. Ramdya, P., Lichocki, P., Cruchet, S., Frisch, L., Tse, W., Floreano, D., and Benton, R. (2015). Mechanosensory interactions drive collective behaviour in *Drosophila*. Nature *519*, 233–236.
23. Chen, T.-W., Wardill, T.J., Sun, Y., Pulver, S.R., Renninger, S.L., Baohan, A., Schreiter, E.R., Kerr, R.A., Orger, M.B., Jayaraman, V., et al. (2013). Ultrasensitive fluorescent proteins for imaging neuronal activity. Nature *499*, 295–300.
24. Sweeney, S.T., Broadie, K., Keane, J., Niemann, H., and O'Kane, C.J. (1995). Targeted expression of tetanus toxin light chain in *Drosophila* specifically eliminates synaptic transmission and causes behavioral defects. Neuron *14*, 341–351.

Current Biology, Volume *27*

Supplemental Information

Moonwalker Descending Neurons Mediate Visually Evoked Retreat in *Drosophila*

Rajyashree Sen, Ming Wu, Kristin Branson, Alice Robie, Gerald M. Rubin, and Barry J. Dickson

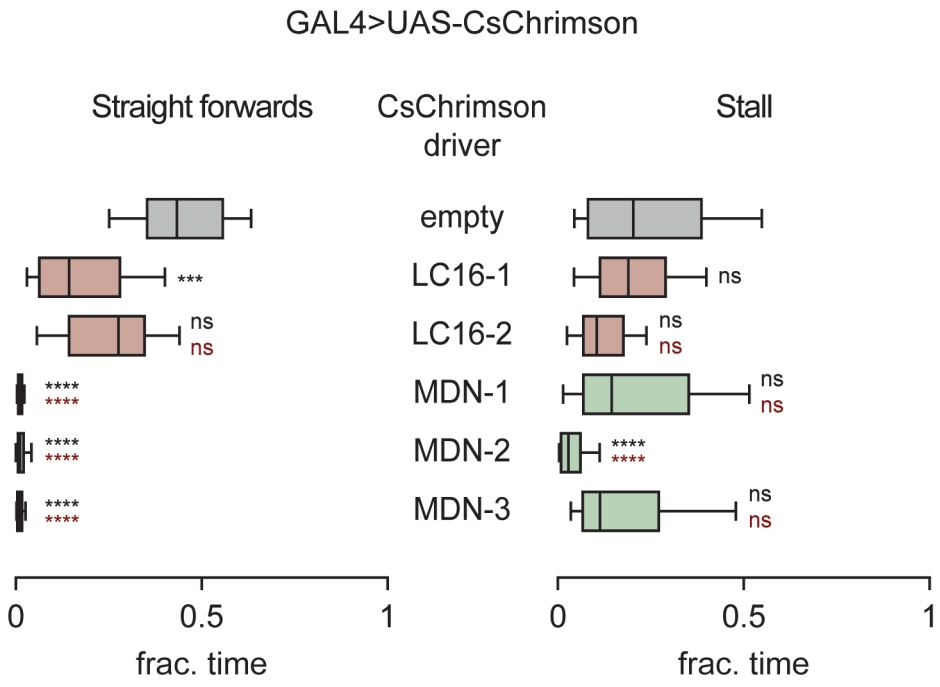

Figure S1. Fraction of time in forwards straight and stalled states upon optogenetic neuronal activation of LC16 or MDN cells. Related to Figure 1.

Per-fly mean over 5 trials, of fraction of time spent in forwards straight and stalled behavioral states during the 2 s window of optogenetic activation. Kruskal-Wallis tests ($P < 0.0001$ for both states) were followed by Dunn's post-hoc test for pairwise comparisons against empty GAL4 (black) and LC16-1 (red) controls.

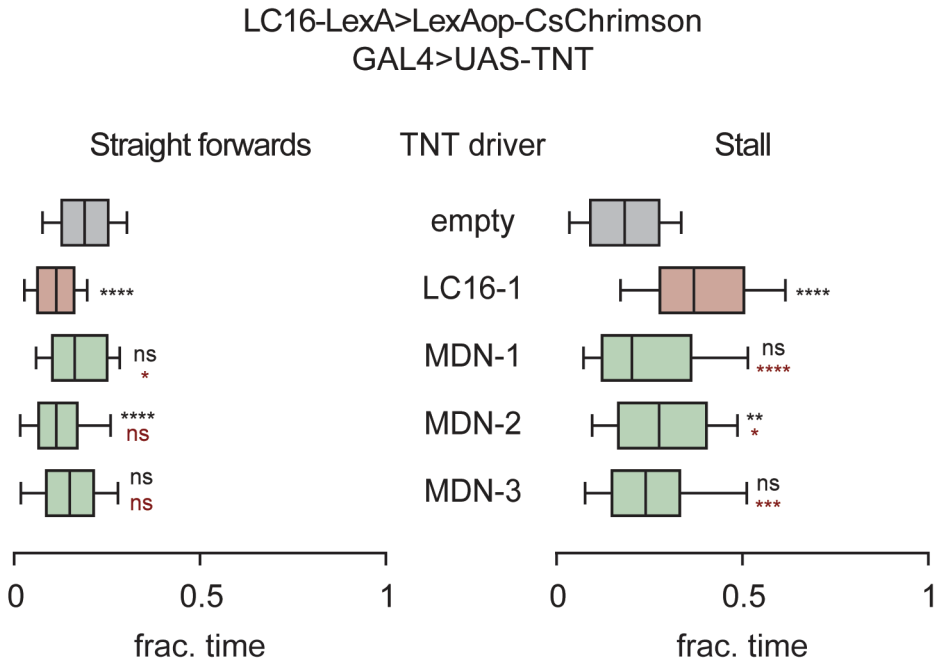

Figure S2. Fraction of time in forwards straight and stalled states in neuronal epistasis experiments. Related to Figure 3.

Per-fly mean over 5 trials, of fraction of time spent in forwards straight and stalled behavioral states during the 2 s window of optogenetic activation of LC16 cells. Kruskal-Wallis tests ($P < 0.0001$ for both states), were followed by Dunn's post-hoc test in pairwise comparisons against the negative (empty, black) and positive (LC16-1, red) controls.

GAL4:	None	*LC16-2*	*LC16-1*	*LC16-1* (mec)	*LC16-1* (wash-out)
	Mean±SEM	Mean±SEM	Mean±SEM	Mean±SEM	Mean±SEM
fly#1	0.14±0.03	0.42±0.04	0.49±0.05	0.10±0.04	0.13±0.02
fly#2	0.14±0.03	0.53±0.04	0.53±0.04	0.07±0.01	0.23±0.04
fly#3	0.13±0.03	0.06±0.02	0.50±0.03	0.15±0.04	0.16±0.03
fly#4	0.10±0.03	0.21±0.02	0.51±0.07	0.12±0.03	0.23±0.04
fly#5	0.16±0.02	0.43±0.05	0.31±0.05	0.05±0.02	0.23±0.02
fly#6	0.07±0.03	0.41±0.04	0.30±0.03		
fly#7	-0.01±0.01		0.42±0.02		
fly#8	0.06±0.01		0.72±0.09		

Table S1. Per-fly means of average $\Delta F/F_0$ in MDNs upon optogenetic stimulation of LC16 cells. Related to Figure 2.
For each fly carrying the indicated split-GAL4 driver together with *UAS-CsChrimson MDN-LexAp65 LexAop-GCaMP6m*, the mean $\Delta F/F_0$ in MDNs during each trial of LC16 activation was calculated. The mean of these per-trial mean $\Delta F/F_0$ values (over 20 trials) yielded the per-fly means tabulated above.

GAL4 driver	*n*	Mean±SEM	Median
None	8	0.10±0.02	0.12
LC16-2	6	0.34±0.07	0.41
LC16-1	8	0.47±0.05	0.49
LC16-1 (With MEC)	5	0.07±0.02	0.07
LC16-1 (MEC Wash-out)	5	0.20±0.02	0.23

Table S2. Mean of per-fly means of average $\Delta F/F_0$ in MDNs upon optogenetic activation of LC16 cells. Related to Figure 2.
Per-fly means of $\Delta F/F_0$ values, calculated as described above, were averaged over all flies of a given genotype; *n* indicates the number of flies tested for each genotype.

Supplemental Experimental Procedures

List of genotypes

Figure	Genotype	Driver(s)
Figure 1A	20XUAS-CsChrimson-mVenus (attP18); R26A03-p65ADZp (attP40)/+; R54A05-ZpGAL4DBD (attP2)/+	LC16-1-GAL4
	20XUAS-CsChrimson-mVenus (attP18); 037220-p65ADZp (attP40)/+; 044845-ZpGAL4DBD (attP2)/+	MDN-2-GAL4
Figure 1B,C,D	20XUAS-CsChrimson-mVenus (attP18); ; pBDPGAL4 (attP2)/+	empty
	20XUAS-CsChrimson-mVenus (attP18); R26A03-p65ADZp (attP40)/+; R54A05-ZpGAL4DBD (attP2)/+	LC16-1-GAL4
	20XUAS-CsChrimson-mVenus (attP18); R82D11-p65ADZp (attP40)/+; R54A05-ZpGAL4DBD (attP2)/+	LC16-2-GAL4
	20XUAS-CsChrimson-mVenus (attP18); 044845-ZpGAL4DBD (attP40)/+; 050660-p65ADZp (attP2)/+	MDN-1-GAL4
	20XUAS-CsChrimson-mVenus (attP18); 037220-p65ADZp (attP40)/+; 044845-ZpGAL4DBD (attP2)/+	MDN-2-GAL4
	20XUAS-CsChrimson-mVenus (attP18); 050660-p65ADZp (attP40)/+; 044845-ZpGAL4DBD (attP2)/+	MDN-3-GAL4
Figure 2B,C	5XUAS-CsChrimson-mCherry (su(Hw)attP5), 044845-LexAp65 (attP40)/+; LexAop2-IVS-GCaMP6m-p10 (VK00005)/+	MDN-LexAp65 (none)
	5XUAS-CsChrimson-mCherry (su(Hw)attP5), 044845-LexAp65 (attP40)/R26A03-p65ADZp (attP40); LexAop2-IVS-GCaMP6m-p10 (VK00005)/R54A05-ZpGAL4DBD (attP2)	LC16-1-GAL4, MDN-LexAp65
	5XUAS-CsChrimson-mCherry (su(Hw)attP5), 044845-LexAp65 (attP40)/R82D11-p65ADZp (attP40); LexAop2-IVS-GCaMP6m-p10 (VK00005)/R54A05-ZpGAL4DBD (attP2)	LC16-2-GAL4, MDN-LexAp65
Figure 3A	13XLexAop2-IVS-CsChrimson-mVenus (attP18); 26A03-LexAp65 (JK22C)/+; pJFRC35-10XUAS-DSCP-E86tetLC (VK00005)/pBDPGAL4 (attP2)	pBDPGAL4 (empty), LC16-LexAp65
	13XLexAop2-IVS-CsChrimson-mVenus (attP18); 26A03-LexAp65 (JK22C)/050660-p65ADZp (attP40); pJFRC35-10XUAS-DSCP-E86tetLC (VK00005)/044845-ZpGAL4DBD (attP2)	MDN-3-GAL4, LC16-LexAp65
Figure 3B,C,D	13XLexAop2-IVS-CsChrimson-mVenus (attP18); 26A03-LexAp65 (JK22C)/+; pJFRC35-10XUAS-DSCP-E86tetLC (VK00005)/pBDPGAL4 (attP2)	pBDPGAL4 (empty), LC16-LexAp65
	13XLexAop2-IVS-CsChrimson-mVenus (attP18); 26A03-LexAp65	LC16-1-

	(JK22C)/R26A03-p65ADZp (attP40); pJFRC35-10XUAS-DSCP-E86tetLC (VK00005)/R54A05-ZpGAL4DBD (attP2)	GAL4, LC16-LexAp65
	13XLexAop2-IVS-CsChrimson-mVenus (attP18); 26A03-LexAp65 (JK22C)/044845-ZpGAL4DBD (attP40); pJFRC35-10XUAS-DSCP-E86tetLC (VK00005)/050660-p65ADZp (attP2)	MDN-1-GAL4, LC16-LexAp65
	13XLexAop2-IVS-CsChrimson-mVenus (attP18); 26A03-LexAp65 (JK22C)/037220-p65ADZp (attP40); pJFRC35-10XUAS-DSCP-E86tetLC (VK00005)/044845-ZpGAL4DBD (attP2)	MDN-2-GAL4, LC16-LexAp65
	13XLexAop2-IVS-CsChrimson-mVenus (attP18); 26A03-LexAp65 (JK22C)/050660-p65ADZp (attP40); pJFRC35-10XUAS-DSCP-E86tetLC (VK00005)/044845-ZpGAL4DBD (attP2)	MDN-3-GAL4, LC16-LexAp65
Figure 4	pJFRC300-20XUAS-FRT>-dSTOP-FRT>-CsChrimson-mVenus (attP18), hs-FLP-PESTOpt (attP3)/+; 044845-ZpGAL4DBD (attP40)/+; 050660-p65ADZp (attP2)/+	MDN-1-GAL4

Fly genetics

The *LC16-LexAp65 and MDN-LexAp65* lines were derived respectively from the *26A03-GAL4* and *VT044845-GAL4* lines by gateway cloning, and correspondingly inserted into the JK22C [S1] and attP40 [S2] landing sites by phiC31-mediated recombination. These lines reliably targeted the LC16 and MDN cell populations and could recapitulate the corresponding activation phenotypes established with GAL4 and split-GAL4 drivers (data not shown). Split-GAL4 driver lines *MDN-1*, *MDN-2* and *MDN-3* were as described in [S3], and *LC16-1* and *LC16-2* correspond to *0L0046B* and *0L0017B*, respectively, as described in [S4]. Other stocks used were (1) *pJFRC35-10XUAS-DSCP-E86tetLC* (VK00005), abbreviated as *UAS-TNT*, a gift from Barret Pfeiffer; (2) *13XLexAop2-IVS-CsChrimson-mVenus* (attP18), Bloomington stock #55137 [S5]; (3) *20XUAS-CsChrimson-mVenus* (attP18) [S5]; (4) *hs-FLP-PESTOpt* (attP3) [S6]; (5) *pJFRC300-20XUAS-FRT>-dSTOP-FRT>-CsChrimson-mVenus* (attP18) [S4], *pBPDGAL4U* (attP2) [S7]; (6) *5XUAS-CsChrimson-mCherry* (su(Hw)attP5), a gift from Vivek Jayaraman; (7) *LexAop2-IVS-GCaMP6m-p10* (VK00005), Bloomington stock #44276 [S8].

All flies were raised in the dark at 50% relative humidity on standard cornmeal-molasses food, supplemented with all-trans-retinal (0.2 mM prior to eclosion, and 0.4 mM post-eclosion).

For activation with CsChrimson, epistasis and calcium imaging experiments, flies were raised at 25°C and aged for 5-7 days before testing. For the stochastic activation experiments, animals were heat-shocked during the 1st instar larval stage and reared at 22°C as described in [S4], with the following modifications: flies were either heat-shocked once for 2 hours, or twice for 2 hours with a 2-hour time interval in between, and were aged for 13-15 days, prior to testing.

Behavioral assays and analysis

All behavioral experiments were performed at 25°C and 50% relative humidity in the dark. The fly chamber used in the assays was designed after previously published works [S9-S11] and consists of an arena within which the flies are constrained in their movements to a plane in which they can be continuously monitored. For optogenetic activation of neurons with CsChrimson, the entire arena was uniformly illuminated with 627 nm LEDs (Red-Orange LUXEON Rebel LED – l22 lm; Luxeon Star LEDs) through a 3 mm thick diffuser. Flies were allowed to walk freely for 1-2 mins before start of the first activation trial. Behavior was recorded under backlit transmitted infrared (IR) 850nm LEDs (Osram SFH 4050) using a camera (ROHS 1.3 MP B&W Flea3 USB 3.0 Camera; POINT GREY) with a 760 nm long-pass filter (NEEWER IR filter, 52 mm) at 30 frames per second (fps) and 1024x1024 pixel resolution. For activation using CsChrimson and in epistasis experiments, groups of ~20 male flies were loaded in the

arena and illuminated with red light of intensity ~5.6 mW/cm^2, for five trials. Each trial comprised a 2 s light stimulus followed by a 20 s light-off period. In the stochastic activation experiments, flies of both sexes were tested individually for fifteen trials, with a light intensity of ~20.1 mW/cm^2. Each trial comprised a 5 s light stimulus, followed by a 20 s light-off period. Individual flies were retrieved for post-hoc histology. During the light stimulations, control flies experienced an initial startle response and either moved faster (activation experiments) or moved slower (stochastic activation experiments) depending on the intensity of light.

Videos of freely walking flies were tracked with a modified version of Ctrax [S9] that used wing shape to determine the orientation of flies. Only flies with complete or continuous tracking throughout the videos were considered for analysis. For each trial, we analyzed a time window that centered on the duration of red-light illumination. This was 6 s total (2 s each before, during and after stimulus) for the activation and epistasis experiments, and 15 s total (5 s each before, during and after stimulus) for the stochastic activation experiments. The tracking fits an ellipse to the fly, and angular velocity and forward velocity for every frame were calculated as in [S11]. Angular velocity was defined as the change in the body angle relative to the global coordinate system. Positive and negative values for angular velocity indicated right and left turns respectively. Forward velocity (for simplicity, referred to as 'translational velocity' in figures) was the projection of the fly's velocity on its orientation direction. We linearly interpolated the time-points when forward velocity became 0 mm/sec. 'Backward translation' distance was calculated as the total integrated area from the interpolated time-series plots whenever forward velocity was negative. Total 'rotation angle' for the epistasis and activation experiments was calculated by integrating the area under the angular velocity (i.e., |angular velocity|) vs. time plots. For the stochastic activation experiments, we linearly interpolated the time-points when angular velocity became 0 rad/s and separately calculated the total angles turned left and right in each trial for a given fly. Turns from the cases where more right MDN cells were labeled were sign-reversed and converted into right turns. We thus defined 6 distinct categories: (1) no MDN cells, (2) 1 cell on one side, (3) 2 cells on one side, (4) 1 cell on each side, (5) 2 cells on each side, and (6) 3 cells, with 2 on one side and 1 on the other. We pooled data from all flies of a given category of expression pattern, and defined turning indices as the ratio of contralateral/(contralateral+ipsilateral) angular distances (with respect to the side where more MDN cells were labeled) for the asymmetric classes, and right/(left+right) angular distances for the symmetric/no labeling classes. We separately calculated the mean turning indices before and during stimulation for each fly over fifteen trials, and defined a per-fly 'turning-bias index', which was the mean subtracted turning index between light on and off.

For analyses of behavioral states, we manually annotated a subset of the data when the flies were in a given walking mode. Treating these classifications as ground-truth, we used hysteresis-based thresholds [S12, S13] on translational and angular velocities for a given behavioral state. A behavioral bout began when velocity increased beyond an upper threshold and ended when it fell below a lower threshold. Short bouts and pauses (<3 frames, or <100 ms at 30 fps) were removed and merged with the fly's state in neighboring frames. Frames in which angular or translational velocity exceeded 50 units/s or dipped below -50 units/s were recognized as jumps and eliminated from the analyses [S12]. A backward locomotion bout began when translational velocity fell below a threshold of -1.75 mm/s and ended when it rose above a threshold of -1.5 mm/s. A forward locomotion bout began when translational velocity exceeded 2 mm/s and ended when it fell below 1.5 mm/s. A turning bout began when angular velocity exceeded 2 rad/s and ended when it dipped below a lower threshold of 1.75 rad/s. Thus, periods when angular velocity fell below 1.75 rad/s were considered as 'not turning' and periods when translational velocity varied between -1.5 mm/s and 1.5 mm/s were considered as 'not translating'. These thresholds thus defined the 6 behavioral states of stalled (neither translating nor turning), pivot (turning without translation), forwards or backwards straight (translating without turning), and forward or backward turn (both translating and turning). Fraction of time spent in each of these behavioral states was calculated as the trial-averaged ratio of the total number of frames the flies spent in the given state to the total number of frames in the respective optogenetic trial. Fraction-time for 'total backward locomotion' was defined as the sum of the fraction-times for 'straight backwards' and 'backward turns'.

Immunohistochemistry and imaging

Immunohistochemistry of the first batch of stochastic activation experiments was performed as described in [S14] with minor modifications: flies were fixed overnight at 4°C in 1.2% PFA, and the central nervous systems (CNSs) were stained with rabbit anti-GFP (1:500, Invitrogen), mouse mAb nc82 (1:50, Hybridoma Bank) and secondary Alexa 488 and 647 antibodies (1:300, Life Technologies). Subsequent batches used a higher throughput immunohistochemistry protocol, as described in https://www.janelia.org/sites/default/files/Project%20Teams/Fly%20Light/FL%20Protocol%20-%20Adult%20IHC%20-%20Split%20Screen_0.pdf. Confocal stacks of the stained brains and ventral nerve cords were acquired with a Zeiss LSM 710 with a 20X air objective. Movie S2 showing overlaid segmentations of LC16 neurons and MDNs onto common reference template was generated using Fluorender [S15], a 3D image rendering software.

Calcium imaging and analysis

The CNSs of female flies were dissected using minimal illumination - in extracellular solution containing (in millimoles): 103 NaCl, 3 KCl, 5 N-Tris (hydroxymethyl) methyl-2-aminoethanesulfonic acid, 10 trehalose, 10 glucose, 2 sucrose, 26 $NaHCO_3$, 1 NaH_2PO_4, 1.5 $CaCl_2$, and 4 $MgCl_2$ (pH near 7.3 when bubbled with 95% (vol/vol) O_2 and 5% (vol/vol) CO_2, ~295 mOsm). We used female flies because *MDN-LexAp65* labeled MDN cells more strongly in females. Imaging was done using a 2-photon scanning microscope (Zeiss MP710), with a 20X water immersion objective of N.A. 1 (Objective W Plan-Apochromat) at a wavelength of 920 nm and an image acquisition frequency of 2 Hz. Throughout the experiment, the sample was perfused in saline bubbled with 95% O_2 (v/v) and 5% CO_2 (v/v) at a speed of ~80-100 ml/hour. The imaging plane spanned the entire area of the brain with an optical slice in which we could reliably identify MDN dendritic arbors on both sides of the brain. An LED (660 nm) light-source collimated with an optic fiber of diameter 400 µm and N.A. 0.39 was used to activate CsChrimson. The location of the optic fiber with respect to the brain was controlled by a micromanipulator targeting the center of the brain. The distance between the sample and the optic fiber ranged from 0.5-1 mm. Light powers were measured directly from the LED light source using a power-meter (Thorlabs). Intensity measures ranged from 1.06-2.17 mW/mm^2 for an imaging plane 0.5-1 mm away from the source. Each trial comprised 5 s of continuous red light stimulation, followed by 35 s of light-off period. Each fly was tested for 10 trials. For blocking nicotinic transmission, 10-15 µl of mecamylamine stock (5 mM) was added directly to a ~5 ml static bath to generate a final concentration of 10-15 µM. Perfusion was stopped for ~10 mins to allow time for action. Preliminary experiments established that stopping the perfusion alone does not eliminate responses in MDNs. For wash-out experiments, samples were perfused with ~50 ml of saline prior to imaging.

For analysis, regions of interest (ROIs) on MDN dendrites from left and right sides of brain were hand-drawn in Fiji (http://fiji.sc). The ROIs were located in the lower lateral accessory lobe (LLAL), near the lateral accessory lobe commissure (LALC). This brain region could be reliably identified from the baseline GCaMP6m signal and by using the location of other neurons labeled in the *MDN-LexAp65* driver line as landmarks. The areas of the left and right ROIs were kept the same for all flies. Absolute fluorescence was calculated as the average pixel intensity in each ROI, for every frame of the video. $\Delta F/F_0$ (F_0 is the average signal over 10 s before the stimulation) was calculated for each video in these ROIs. Data from the left and right ROIs were pooled together since MDN has symmetric dendritic arborizations in the brain. For each trial, the average $\Delta F/F_0$ values over the 5 s red light stimulation was calculated, and the mean of these average $\Delta F/F_0$ over 20 trials yielded a per-fly mean.

Supplemental References

S1. Knapp, J.M., Chung, P., and Simpson, J.H. (2015). Generating customized transgene landing sites and multi-transgene arrays in *Drosophila* using phiC31 integrase. Genetics *199*, 919-934.

S2. Markstein, M., Pitsouli, C., Villalta, C., Celniker, S.E., and Perrimon, N. (2008). Exploiting position effects and the gypsy retrovirus insulator to engineer precisely expressed transgenes. Nat. Genet. *40*, 476-483.

S3. Bidaye, S.S., Machacek, C., Wu, Y., and Dickson, B.J. (2014). Neuronal control of *Drosophila* walking direction. Science *344*, 97-101.

S4. Wu, M., Nern, A., Williamson, W.R., Morimoto, M.M., Reiser, M.B., Card, G.M., and Rubin, G.M. (2016). Visual projection neurons in the *Drosophila* lobula link feature detection to distinct behavioral programs. eLife *5*, e21022.

S5. Klapoetke, N.C., Murata, Y., Kim, S.S., Pulver, S.R., Birdsey-Benson, A., Cho, Y.K., Morimoto, T.K., Chuong, A.S., Carpenter, E.J., Tian, Z., et al. (2014). Independent optical excitation of distinct neural populations. Nat. Methods *11*, 338-346.

S6. Nern, A., Pfeiffer, B.D., and Rubin, G.M. (2015). Optimized tools for multicolor stochastic labeling reveal diverse stereotyped cell arrangements in the fly visual system. Proc. Natl. Acad. Sci. U S A *112*, E2967-2976.

S7. Pfeiffer, B.D., Ngo, T.T., Hibbard, K.L., Murphy, C., Jenett, A., Truman, J.W., and Rubin, G.M. (2010). Refinement of tools for targeted gene expression in *Drosophila*. Genetics *186*, 735-755.

S8. Chen, T.-W., Wardill, T.J., Sun, Y., Pulver, S.R., Renninger, S.L., Baohan, A., Schreiter, E.R., Kerr, R.A., Orger, M.B., Jayaraman, V., et al. (2013). Ultrasensitive fluorescent proteins for imaging neuronal activity. Nature *499*, 295-300.

S9. Branson, K., Robie, A.A., Bender, J., Perona, P., and Dickinson, M.H. (2009). High-throughput ethomics in large groups of *Drosophila*. Nat. Methods *6*, 451-457.

S10. Simon, J.C., and Dickinson, M.H. (2010). A new chamber for studying the behavior of *Drosophila*. PLoS ONE *5*, e8793.

S11. Kabra, M., Robie, A.A., Rivera-Alba, M., Branson, S., and Branson, K. (2013). JAABA: interactive machine learning for automatic annotation of animal behavior. Nat Methods *10*, 64-67.

S12. Robie, A.A., Straw, A.D., and Dickinson, M.H. (2010). Object preference by walking fruit flies, *Drosophila melanogaster*, is mediated by vision and graviperception. J. Exp. Biol. *213,* 2494-2506.

S13. Ramdya, P., Lichocki, P., Cruchet, S., Frisch, L., Tse, W., Floreano, D., and Benton, R. (2014). Mechanosensory interactions drive collective behaviour in *Drosophila*. Nature *519*, 233-236.

S14. Yu, J.Y., Kanai, M.I., Demir, E., Jefferis, G.S., and Dickson, B.J. (2010). Cellular organization of the neural circuit that drives *Drosophila* courtship behavior. Curr. Biol. *20*, 1602-1614.

S15. Wan, Y., Otsuna, H., Chien, C.B., and Hansen, C. (2012). FluoRender: An application of 2D image space methods for 3D and 4D confocal microscopy data visualization in neurobiology research. IEEE Pac. Vis. Symp., 201-208.